

# Anomaly Detection of Underwater Gliders Verified by Deployment Data

Ruochu Yang

*School of Electrical and Computer Engineering  
Georgia Institute of Technology  
Atlanta, United States*

Mengxue Hou

*College of Engineering  
Purdue university  
West Lafayette, United States*

Chad Lembke

*College of Marine Science  
University of South Florida  
St.Petersburg, United States*

Catherine Edwards

*Skidaway Institute of Oceanography  
University of Georgia  
Savannah, United States*

Fumin Zhang

*School of Electrical and Computer Engineering  
Georgia Institute of Technology  
Atlanta, United States*

**Abstract**—This paper utilizes an anomaly detection algorithm to check if underwater gliders are operating normally in the unknown ocean environment. Glider pilots can be warned of the detected glider anomaly in real time, thus taking over the glider appropriately and avoiding further damage to the glider. The adopted algorithm is validated by two valuable sets of data in real glider deployments, the University of South Florida (USF) glider Stella and the Skidaway Institute of Oceanography (SkIO) glider Angus.

**Index Terms**—anomaly detection, glider navigation

## I. INTRODUCTION

Autonomous underwater profiling gliders, hereafter referred to as gliders, have been widely used in oceanography for a range of applications, including harmful algal bloom monitoring, improving hurricane prediction, passive and active acoustics, ocean observing systems, and targeted science questions [1]–[5]. Similar progress has been made to improve the performance and value of the data collected through coordinated control of vehicles over long

durations [6]–[8]. Despite these advances, unpredictable events like shark or vessel strikes [9], wing loss, or interaction with echneids (remoras) can lead to abnormal flight behavior, prematurely end a glider’s mission, or even result in the loss of the vehicle. Human pilots cannot always directly track gliders’ abnormal behavior from the subsets of measured data that are telemetered to shore, especially when gliders confront external disturbances [10], [11], and sending more data or adding monitoring devices to detect abnormal behavior is not always feasible or helpful. Therefore, anomaly detection algorithms can be developed to aid human pilots, and their design must rely on a limited subset of glider data.

Anomaly detection has been studied extensively in the robotics community [12]–[14]. Specifically in the domain of marine robots, some anomaly detection algorithms focus on individual components that frequently degrade like propellers, thrusters, and rotors [15]–[18]. Other anomaly detection algorithms utilize robot motion like monitoring pitch angle and depth angle to detect possible deviation from expected motion [19]. However, research to date has not yet resolved issues such as inaccessible hardware

The research work is supported by ONR grants N00014-19-1-2556 and N00014-19-1-2266; AFOSR grant FA9550-19-1-0283; NSF grants GCR-1934836, CNS-2016582 and ITE-2137798; and NOAA grant NA16NOS0120028.

dynamics, incapability of performing online detection, and lack of experimental verification. Detected anomalies must also be checked against the case of false alarm [20]. One common scenario occurs when flow speed exceeds the maximum robot speed; the performance of marine robots is degraded in terms of speed over the ground [6], but the anomaly occurs due to environmental conditions rather than flight performance of the robot itself. Therefore, it is significant to compare marine robot speed with ocean flow speed; this comparison is not trivial since flow speed is not directly measured by the glider but is instead estimated through dead reckoning.

Controlled Lagrangian particle tracking (CLPT) is a theoretical framework that can simultaneously estimate ocean flow speed and robot speed [21]. Based on these two estimates, it is feasible to detect abnormal motion while providing robust false alarm avoidance by excluding unexpected ocean flow. The anomaly detection algorithm applied in this paper is adopted from the work [22], which uses trajectory data and heading angle data that are available and generic in all types of gliders. This similar technique of leveraging glider navigational data can also be seen in previous work [23]–[25]. Given a trajectory and heading angles, the adopted algorithm generates both the estimated flow speed and the estimated glider speed in real time. The estimated glider speed can be compared with the normal speed range to check for anomalies, and the estimated flow speed is compared with the glider-estimated flow speed to check if the detected anomaly is a false alarm.

In general, anomaly detection is difficult to validate in field experiments. In abnormal conditions, gliders are likely to encounter issues of GPS search, thus imposing risk and cost to human rescue. Anomalies occur unexpectedly, there is lack of “ground truth” to determine the major factor causing the anomaly. Further, anomalies can accumulate over time, and it can be difficult for glider pilots to notice in real time even with close monitoring during field experiments. Given only a subset of data, small changes in flight performance can be too subtle for pilots to identify. The main contribution of this paper is to verify the anomaly detection algorithm in [22] using real-life glider deployment data for the first time. The algorithm can infer whether or not the glider may have had a shark

hit, wing loss, or remora attachment simply from a subset of flight data rather than large amounts of data. The University of South Florida (USF) glider Stella and the Skidaway Institute of Oceanography (SkIO) glider Angus provide two valuable sets of experimental data, in which anomalies can be attributed to marine bio-hazards and strong evidence is available to confirm their cause. Both data sets show promising detection results to validate the anomaly detection algorithm in [22].

This paper is organized as follows. Section II describes the working principles of Slocum glider and the experiment setup of two coastal glider deployments in the Gulf of Mexico and south east Atlantic Ocean. Section III illustrates the framework of the anomaly detection algorithm. Section IV verifies the algorithm by showing results of detected anomalies. Section V provides conclusions and future work.

## II. GLIDER AND EXPERIMENT SETUP

This section introduces the Slocum glider, its method of navigation, and the details of deployments of two gliders, Stella and Angus, that were subjected to anomalous conditions while deployed.

### A. Slocum Glider

The Slocum glider is an autonomous underwater vehicle (AUV) that moves by changing its buoyancy and center of gravity [26]. Capable of collecting data in the ocean for long duration missions of up to 6 months without a recharge, gliders typically travel at low speed (approximately  $0.25\text{--}0.35\text{ m} \cdot \text{s}^{-1}$ ). During the deployment, the glider surfaces at pre-defined intervals to transmit flight and science data, as well as receive updates and other instructions via satellite connection. In order to minimize time at the surface, where the glider is vulnerable to ship traffic and other dangers, only a small portion of heavily subsetting flight data are telemetered to shore in small binary data (SBD) files. For example, in The trajectory and heading information of sbd file data is processed in real time by the anomaly detection algorithm presented in Section III. After the mission is over, all the full data sets are downloaded off the glider into Dinkum binary files (DBD and EBD for flight and science data, respectively). The anomaly detection algorithm is validated in Section IV by comparing the anomaly detected from the real-time

SBD file date with the anomaly directly shown from the full DBD file data.

While in mission, the glider estimates its horizontal position using pitch and depth data through dead reckoning. From one surfacing to the next, the deviation the glider makes from the dead reckoned estimate is attributed to the influence of flow. The difference between these two positions are used to estimate the average flow speed along the glider trajectory. GPS positions at the beginning and end of the surfacing are used to adjust the effect of surface wind drift on estimated flow velocity. This glider-estimated flow is checked against the flow estimate given by the anomaly detection algorithm in Section III.

### B. Field Deployments

Data from two gliders will be used for field validation of the detection anomaly algorithm: the glider Stella, operated by the University of South Florida, and the glider Angus, operated by Skidaway Institute of Oceanography, part of the University of Georgia. Stella (#772) was deployed by the University of South Florida in the Gulf of Mexico on the West Florida Shelf near  $(27.6970^\circ N, 83.8778^\circ W)$  on July 01, 2021 UTC, transited offshore and then back inshore, and ended at the location  $(27.7318^\circ N, 83.4136^\circ W)$  on July 19, 2021 UTC. The Google Earth trajectory of Stella is shown in Fig. 1.



Fig. 1: Google Earth trajectory of the 2021 Stella deployment.

As part of an acoustic telemetry and navigation experiment, the glider Angus was deployed near Gray's Reef National Marine Sanctuary. Its navigation was supported by the Glider Environment Networked Information system (GENIoS) [27], which

generated optimal waypoints for the glider to use based on real-time glider-estimated currents and position at each surfacing. The mission started at the location  $(31.4633^\circ N, 80.7757^\circ W)$  at April 04, 2022, 15:30 UTC, and ended at the location  $(31.5072^\circ N, 80.7368^\circ W)$  at April 25, 2022, 18:51 UTC. The Google Earth trajectory of Angus is shown in Fig. 2.

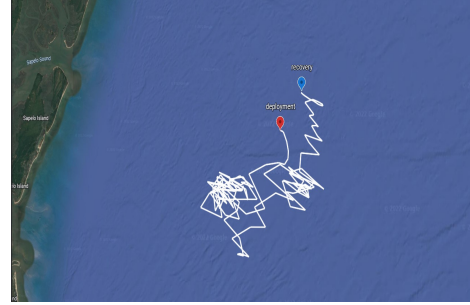


Fig. 2: Google Earth trajectory of the 2022 Angus deployment.

### III. ANOMALY DETECTION ALGORITHM

The adopted anomaly detection algorithm can simultaneously generate glider speed estimate and flow speed estimate in real time. If the glider speed estimate is within the normal speed range, it is assumed that no anomaly has occurred. Otherwise, the glider may not be operating normally. The algorithm-estimated flow speed is compared with glider-estimated flow speed to compute flow estimation error. If the error is too large, the detected anomaly is false alarm. This section illustrates the main framework of anomaly detection algorithm. More theoretical details can be found in the work [22].

The glider motion model is shown in (1),

$$\begin{aligned} \dot{x} &= F_R(x, t) + V_R(t)\Psi_c(t) \\ \Psi_c(t) &= [\cos \psi_c(t), \sin \psi_c(t)]^T \end{aligned} \quad (1)$$

where  $F_R$  is the actual flow field,  $x$  is the true glider position,  $V_R$  is the true glider speed, and  $\psi_c$  is the glider heading angle.

In practice, the glider speed is limited due to the glider control input constraint. Equation (1) can be modified as the combination of (2) and (3),

$$\dot{x} = F_R(x, t) + u\Psi_c(t), \quad (2)$$

where

$$u = \begin{cases} V_R, & \text{if } V_R \leq u_0 \\ u_0, & \text{if } V_R > u_0 \end{cases} \quad (3)$$

The maximum glider speed  $u_0$  is determined by the hardware configuration of the glider, as well as the water depth of operation. As shown in (4), the flow field can be represented by spatial and temporal basis functions (specifically Gaussian radial and tidal functions) [28],

$$F_R(x, t) = \theta\phi(x, t) \quad (4)$$

where

$$\theta = \begin{bmatrix} \theta_1 \\ \theta_2 \end{bmatrix} = \begin{bmatrix} \theta_1^1 & \cdots & \theta_1^N \\ \theta_2^1 & \cdots & \theta_2^N \end{bmatrix} \in \mathbb{R}^{2 \times N} \quad (5)$$

is the unknown parameter to be estimated,

$$\phi = [\phi^1(x, t) \quad \cdots \quad \phi^N(x, t)]^T \quad (6)$$

$$\phi^i(x, t) = \exp\left(-\frac{\|x - c_i\|^2}{2\sigma_i^2}\right) \cos(\omega_i t + v_i) \quad (7)$$

is the combined basis function,  $c_i$  is the center,  $\sigma_i$  is the width,  $\omega_i$  is the tidal frequency,  $v_i$  is the tidal phase, and  $N$  is the selected number of basis functions. The heading  $\Psi_c(t)$  and the true trajectory  $x(t)$  are known for all time  $t$  from the sbd file data operationally sent by the glider. Given the true trajectory  $x(t)$ , the adopted algorithm can estimate the unknown parameter  $\theta$  in (4) and the glider speed  $V_R$  in (1) in real time. Define

$$\xi(t) = \begin{bmatrix} \xi_1(t) \\ \xi_2(t) \end{bmatrix} = \begin{bmatrix} \xi_1^1(t) & \cdots & \xi_1^N(t) \\ \xi_2^1(t) & \cdots & \xi_2^N(t) \end{bmatrix} \in \mathbb{R}^{2 \times N} \quad (8)$$

as the estimate of the flow parameter  $\theta$ . Define  $V_L(t)$  as the estimate of the glider speed  $V_R$ . The adopted algorithm can generate converged estimates, i.e.,  $\lim_{t \rightarrow \infty} \xi(t) \rightarrow \theta$  and  $\lim_{t \rightarrow \infty} V_L(t) \rightarrow V_R$  to ensure that the maximum trajectory estimation error (CLLE) converges to zero. The adopted algorithm also designs three gains  $K$ ,  $\bar{\gamma}_1$  and  $\bar{\gamma}_2$  to accelerate the estimating process.

Next, the glider speed estimate  $V_L(t)$  can be used to decide whether anomalies happened or not, and the flow speed estimate  $\xi(t)$  can be used to avoid

false alarm. The adopted algorithm assumes that the maximum glider speed  $V_{max}$  and the minimum glider speed  $V_{min}$  are known beforehand. If the estimated glider speed  $V_L(t) \in [V_{min}, V_{max}]$ , it is assumed that no anomaly happens to the glider. Otherwise, the glider may not be operating normally. In order to avoid false alarm, the adopted algorithm checks the estimated flow speed as well. Let us introduce  $F_L(t)$  as the flow speed estimated by the adopted algorithm, and  $F_M(t)$  as the flow speed estimated by the glider. In practice, prior information like ocean models or sensor measurements can help generate the glider-estimated flow speed  $F_M(t)$ . The algorithm-estimated flow speed  $F_L(t)$  is compared with the glider-estimated flow speed  $F_M(t)$  to determine if the detected anomaly is false alarm or not. Defining  $\|F_M(t) - F_L(t)\|$  as the flow estimation error, the criteria  $p_E$  to evaluate the flow estimation error is given as (9),

$$p_E = \frac{\|F_M(t) - F_L(t)\|}{2\max(\hat{F}_{Lmax}, \hat{F}_{Mmax})} \quad (9)$$

where  $\hat{F}_{Lmax} = \max(\|F_L(\tau)\|_{\tau \in [0, t]})$  is the maximum algorithm-estimated flow speed until time  $t$ , and  $\hat{F}_{Mmax} = \max(\|F_M(\tau)\|_{\tau \in [0, t]})$  is the maximum glider-estimated flow speed until time  $t$ . If  $p_E > \gamma_f$ , the detected anomaly should not be trusted, where  $\gamma_f$  is a false alarm threshold selected beforehand. The pseudo-code is shown in Algorithm 1. For convenience, we introduce  $f_a$  as anomaly detection flag shown in (10).

$$f_a = \begin{cases} 0 & \text{no anomaly} \\ 1 & \text{anomaly detected} \\ 2 & \text{false alarm} \end{cases} \quad (10)$$

#### IV. EXPERIMENTAL RESULTS

For the purpose of validation, the adopted anomaly detection algorithm is applied to two field deployments with verified anomalies in the coastal ocean of the Gulf of Mexico and south east Atlantic Ocean. The estimated glider speed is compared with the maximum and minimum glider speeds to decide if anomalies can be identified. The estimated flow speed is checked against the glider-estimated flow speed to avoid false alarm. For verification, the anomaly detected by the algorithm is compared with



**Algorithm 1** Anomaly Detection

**Input:** Algorithm-estimated flow speed  $F_L(t)$ , glider-estimated flow speed  $F_M(t)$ , false alarm threshold  $\gamma_f$ , estimated glider speed  $V_L(t)$ , maximum glider speed  $V_{max}$ , minimum glider speed  $V_{min}$  **Output:** Anomaly detection flag  $f_a$

```

1:  $\hat{F}_{Lmax} = \max(|F_L(\tau)|, \tau \in [0, t])$ 
2:  $\hat{F}_{Mmax} = \max(|F_M(\tau)|, \tau \in [0, t])$ 
3:  $p_E = \frac{||F_M(t) - F_L(t)||}{2\max(\hat{F}_{Lmax}, \hat{F}_{Mmax})}$ 
4: if  $p_E > \gamma_f$  then
5:    $f_a = 2$ 
6: else if  $V_L(t) > V_{max}$  or  $V_L(t) < V_{min}$  then
7:    $f_a = 1$ 
8: else
9:    $f_a = 0$ 
10: end if

```

the anomaly seen from glider dbd file data and pilot logs. For reference, the designed parameters of the algorithm are shown in TABLE I.

TABLE I: Parameters of Experiments

Parameters	Stella Deployment Data	Angus Deployment Data
number of basis functions N	4	4
width $\sigma_i$	1.3e4	2e4
tidal phase $v_i$	0	0
tidal frequency $\omega_i$	$2\pi e-6$	$2\pi e-6$
gain K	$\begin{bmatrix} 0.003 & 0 \\ 0 & 0.003 \end{bmatrix}$	$\begin{bmatrix} 0.002 & 0 \\ 0 & 0.002 \end{bmatrix}$
gain $\tilde{\gamma}_1$	1e-7	2e-5
gain $\tilde{\gamma}_2$	35e-10	2e-8
false alarm threshold $\gamma_f$	0.6	0.7

**A. Results of Stella Deployment**

Upon recovery July 19th, 2021, the glider Stella missing one of its two detachable wings, and scratches on the glider hull and the shark tooth embedded in the thermoplastic aft glider cowling (Figs. refshark scratch and 3b) suggest a serious shark strike. Glider pilot analysis of the full DBD data post deployment suggests that the shark hit of the glider likely occurred around July 07, 2021,

16:00 UTC when it was descending at about 55m depth. This post-mission analysis shows that the glider went from a  $-4deg$  roll to an  $8deg$  roll, and finally settled back at about a  $0deg$  roll (Fig. 4a and Fig. 4b). The sudden change of roll and the consistent change through the remainder of the deployment suggests that the wing was lost during this process.



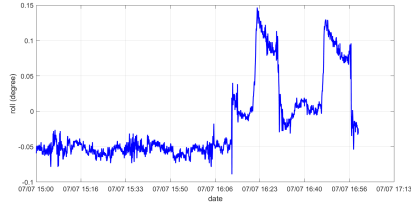
(a) Hull scratches documented after recovery.



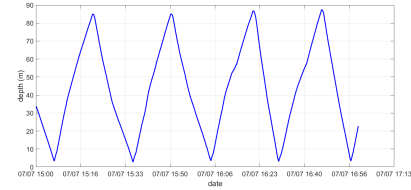
(b) Shark tooth found embedded in the hull after recovery.

Fig. 3: Post-recovery evidence of shark strike.

Applying the anomaly detection algorithm to the telemetered SBD data from the glider, the adopted algorithm can guarantee that the estimated trajectory converges to the true trajectory since the persistent excitation matrix  $W(t)$  is not singular. The comparison of the estimated trajectory with the true trajectory is shown in Fig. 5. It should be noted that the 4 green circles cover the whole trajectory, which means that the 4 combined basis functions cover the whole flow fields. This coverage is necessary for the parameter estimation convergence. As shown in Fig. 6, the maximum trajectory estimation error (CLLE) is only  $1.7m$ , which is small enough considering the glider moved approximately  $0.25m/s$  over  $O(100)km$  in its deployment. Therefore, it can be concluded that the CLLE converges to zero.



(a) Glider-measured roll (degrees) from post-recovery DBD data.



(b) Glider-measured depth (m) from post-recovery DBD data.

Fig. 4: ground truth (Stella deployment).

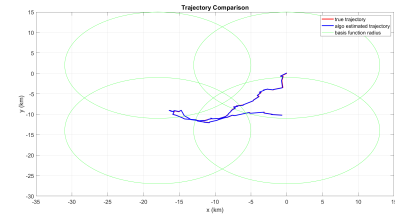


Fig. 5: Comparison of the estimated (blue) and reported “true” (red) trajectory for the 2021 Stella deployment.

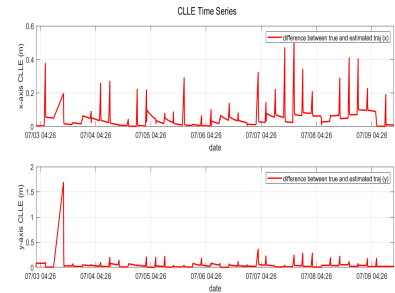
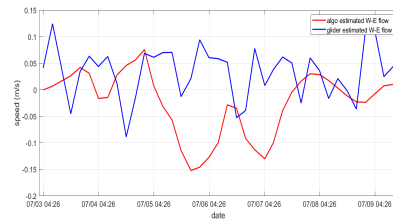
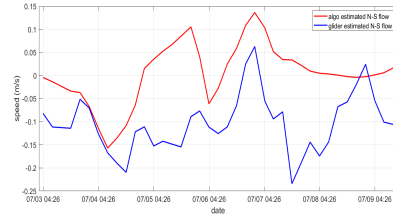


Fig. 6: CLLE (m) for the 2021 Stella deployment.

Given the CLLE convergence, the glider speed estimate and the flow speed estimate should also converge. In this case, the anomaly can be detected based on these two estimates. For better comparison, the flow is divided into  $u$  (West-East, W-E, or zonal) and  $v$  (North-South, N-S, or meridional) components. As shown in Fig. 7a, the algorithm-estimated W-E flow is close to the corresponding glider-estimated W-E flow, which means that the  $u$  flow estimation error is small. Similarly as the N-S flow shown in Fig. 7b. This comparison suggests that the anomaly detection flag can be trusted when it is signaled.



(a) W-E flow component.



(b) N-S flow component.

Fig. 7: Comparison of glider-estimated and algorithm-estimated W-E ( $u$ , upper) and N-S ( $v$ , lower) velocities.

The estimated glider speed is compared with the reported “true” speed value collected by the glider. If the estimated speed is not in the normal speed range, the anomaly is assumed to have occurred. As shown in Fig. 8, the estimated glider speed drops out of the normal speed range (green dot line) at around July 07, 2021, 18:00 UTC, and keeps dropping afterwards. As shown in Fig. 9, the flag value switches from 0 to 1 at around July 07, 2021, 18:00 UTC as well. The flag value never changes to 2 with the false alarm threshold  $\gamma_f = 0.6$ . The timestamp around which the anomaly is detected by the adopted algorithm corresponds to

the timestamp from both the glider team’s report and the full post-deployment DBD file data. Therefore, the adopted algorithm is verified valid and accurate by successfully detecting the anomaly.

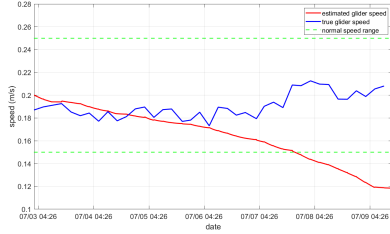


Fig. 8: Comparison of estimated (red) and reported “true” (blue) speed of Stella in the 2021 deployment.

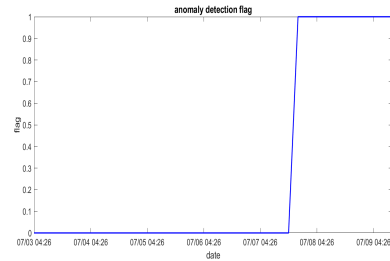


Fig. 9: Anomaly detection flag as calculated by the adopted algorithm for the 2021 Stella deployment.

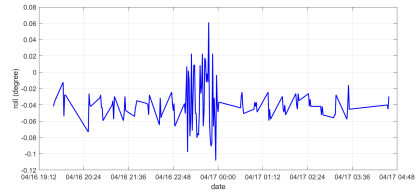
### B. Results of Angus Deployment

According to the mission report, pilots noted that the glider Angus periodically flew slower than expected, and suffered from unusually poor satellite data transmission, with multiple broken connections per surfacing, consistent with remora strikes. The problem was first identified by pilots around April 17, 2022, 00:00 UTC. Since remoras are negatively buoyant, the glider’s Iridium antenna is not fully out of the water, and multiple animals attached to the instrument can induce too much of a buoyancy loss for the glider’s pump to overcome, preventing flight altogether. The remora attachment scene is difficult to catch in real-time missions. For illustration, Fig. 10 shows an example image of two remoras attached to a glider (photo credit: Chad Lembke, College of Marine Science, University of South Florida). Based on the post-recovery DBD file

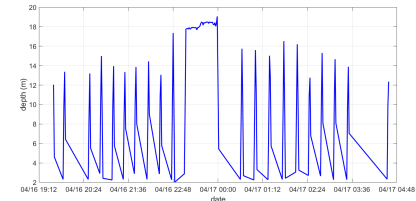
data, the roll and depth ground truth is shown in Fig. 11a and Fig. 11b, respectively. The timestamp April 17, 2022, 00:00 UTC when depth and roll data becomes abnormal exactly matches the glider team’s reported timestamp.



Fig. 10: Example image of remora attachment (photo credit: Chad Lembke, College of Marine Science, University of South Florida).



(a) Glider-measured roll (degrees) from post-recovery DBD data.



(b) Glider-measured depth (m) from post-recovery DBD data.

Fig. 11: ground truth (Angus deployment).

Using the SBD file offloaded from the glider, the calculated persistent excitation matrix  $W(t)$  is not singular, which means that the adopted algorithm can guarantee that the estimated trajectory converges to the true trajectory. The comparison of the estimated trajectory with the true trajectory is shown in Fig. 12. It should be noted that the four green circles

cover the whole trajectory, which means that the four combined basis functions cover the whole flow fields. This coverage is necessary for the parameter estimation convergence. As shown in Fig. 13, the maximum trajectory estimation error (CLLE) only reaches around  $6m$ , which is sufficiently small given the glider speed and range. Therefore, it can be concluded that the CLLE converges to zero.

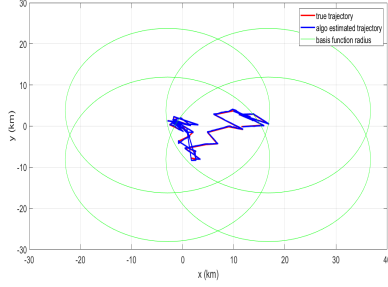


Fig. 12: Comparison of the estimated (blue) and reported “true” (red) trajectory for the 2022 Angus deployment.

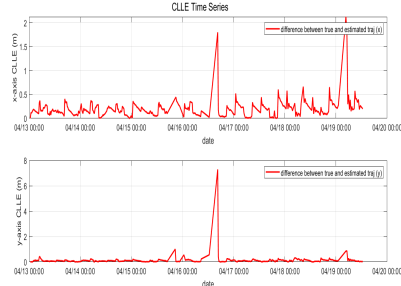
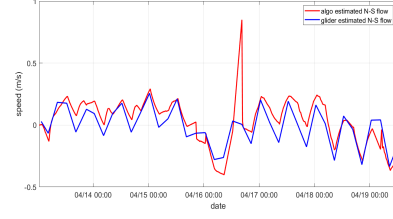
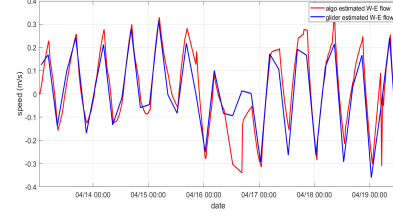


Fig. 13: CLLE (m) for the 2022 Angus deployment.

Given the CLLE convergence, the glider speed estimate and the flow speed estimate should converge as well. In this case, the anomaly can be detected based on these two estimates. For better comparison, the flow is divided into  $u$  (West-East, W-E, or zonal) and  $v$  (North-South, N-S, or meridional) components. As shown in Fig. 14a and 14b, the algorithm-estimated W-E and N-S flow is close to the corresponding glider-estimated values, so both the  $u$  and  $v$  flow estimation errors are small. Therefore, any anomaly detection flag can be trusted.



(a) W-E flow component.



(b) N-S flow component.

Fig. 14: Comparison of glider-estimated and algorithm-estimated W-E ( $u$ , upper) and N-S ( $v$ , lower) velocities.

As shown in Fig. 15, the estimated glider speed sharply drops out of the normal speed range (green dot line) at around April 16, 2022, 22:00 UTC. Afterwards, the glider tries to recover its speed but continues below the normal range. As shown in Fig. 16, the flag value switches from 0 to 1 at around April 16, 2022, 22:00 UTC as well. The flag value never changes to 2 with the false alarm threshold  $\gamma_f = 0.7$ . The timestamp around which the anomaly is detected by the adopted algorithm corresponds to the timestamp from both the glider team’s report and the DBD file data. Therefore, the adopted algorithm is verified valid and accurate, and the anomaly is successfully detected.

## V. CONCLUSION

This paper implements and validates an anomaly detection algorithm for two sets of data in real missions of gliders, the University of South Florida (USF) glider Stella and the Skidaway Institute of Oceanography (SkIO) glider Angus, where the anomalies of shark attack and remora attachment can be verified. Based on the glider trajectory and the heading angle data, the algorithm generates glider speed estimate and flow speed estimate in real time. The estimated glider speed is compared with



Fig. 15: Comparison of estimated speed (red) and normal speed range (green) of Angus in the 2022 deployment.

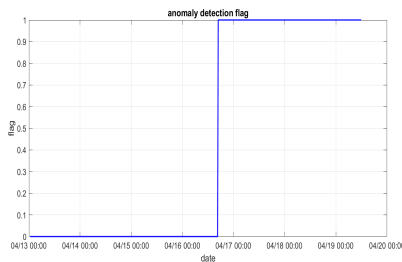


Fig. 16: Anomaly detection flag as calculated by the adopted algorithm for the 2022 Angus deployment.

the normal glider speed range to decide whether anomalies happen or not. The estimated flow speed is compared with the glider-estimated flow speed to determine if the detected anomaly is a false alarm. From a theoretical point of view, the current algorithm focuses on the real-time estimation process by predicting and updating the trajectory, which is known as the filtering framework, as the ongoing deployment gives the real glider data as feedback. Future work will improve the estimation accuracy by integrating the post-deployment glider data as a smoothing framework. From a practical point of view, future work will implement algorithms that account for dependence of glider speed on water depth, and consider the dependency of error on glider heading angle, which can be used to diagnose poor ballasting of the instrument.

#### REFERENCES

- [1] T. N. Miles, D. Zhang, G. R. Foltz, J. A. Zhang, C. Meinig, F. Bringas, J. Triñanes, M. Le Hénaff, M. F. Aristizabal Vargas, S. Coakley *et al.*, “Uncrewed ocean gliders and saildrones support hurricane forecasting and research,” *Oceanography*, vol. 34, no. 4, pp. 78–81, 2021.
- [2] P. Testor, B. de Young, D. L. Rudnick, S. Glenn, D. Hayes, C. M. Lee, C. Pattiaratchi, K. Hill, E. Heslop, V. Turpin, P. Alenius, C. Barrera *et al.*, “Oceangliders: A component of the integrated goos,” *Frontiers in Marine Science*, vol. 6, 2019.
- [3] R. H. Weisberg, Y. Liu, C. Lembke, C. Hu, K. Hubbard, and M. Garrett, “The coastal ocean circulation influence on the 2018 west florida shelf k. brevis red tide bloom,” *Journal of Geophysical Research: Oceans*, vol. 124, no. 4, pp. 2501–2512, 2019.
- [4] P. Cauchy, K. J. Heywood, N. D. Merchant, B. Y. Queste, and P. Testor, “Wind speed measured from underwater gliders using passive acoustics,” *Journal of Atmospheric and Oceanic Technology*, vol. 35, no. 12, pp. 2305–2321, 2018.
- [5] M. F. Baumgartner, J. Bonnell, P. J. Corkeron, S. M. Van Parijs, C. Hotchkin, B. A. Hodges, J. Bort Thornton, B. L. Mensi, and S. M. Bruner, “Slocum gliders provide accurate near real-time estimates of baleen whale presence from human-reviewed passive acoustic detection information,” *Frontiers in Marine Science*, vol. 7, 2020.
- [6] F. Zhang, D. M. Fratantoni, D. A. Paley, J. M. Lund, and N. E. Leonard, “Control of coordinated patterns for ocean sampling,” *International Journal of Control*, vol. 80, no. 7, pp. 1186–1199, 2007.
- [7] D. A. Paley, F. Zhang, and N. E. Leonard, “Cooperative control for ocean sampling: The glider coordinated control system,” *IEEE Transactions on Control Systems Technology*, vol. 16, no. 4, pp. 735–744, 2008.
- [8] H. Hou, S. Cho, H. Zhou, C. R. Edwards, and F. Zhang, “Bounded cost path planning for underwater vehicles assisted by a time-invariant partitioned flow field model,” *Frontiers in Robotics and AI*, vol. 8, 2021.
- [9] M. Stanway, B. Kieft, T. Hoover, B. Hobson, D. Klimov, J. Erickson, B. Raanan, D. Ebert, and J. Bellingham, “White shark strike on a long-range auv in monterey bay,” 05 2015.
- [10] J. J. Gertler, *Fault detection and diagnosis in engineering systems*. CRC press, 2017.
- [11] J. Chen and R. J. Patton, *Robust model-based fault diagnosis for dynamic systems*. Springer Science & Business Media, 2012, vol. 3.
- [12] B.-Y. Raanan, J. G. Bellingham, Y. Zhang, M. Kemp, B. Kieft, H. Singh, and Y. Girdhar, “Automatic fault diagnosis for autonomous underwater vehicles using online topic models,” in *OCEANS 2016 MTS/IEEE Monterey*. IEEE, 2016, pp. 1–6.
- [13] D. Park, Z. Erickson, T. Bhattacharjee, and C. C. Kemp, “Multimodal execution monitoring for anomaly detection during robot manipulation,” in *2016 IEEE International Conference on Robotics and Automation (ICRA)*. IEEE, 2016, pp. 407–414.
- [14] R. Isermann, “Model-based fault-detection and diagnosis—status and applications,” *Annual Reviews in control*, vol. 29, no. 1, pp. 71–85, 2005.
- [15] G. Fagogenis, V. De Carolis, and D. M. Lane, “Online fault detection and model adaptation for underwater vehicles in the case of thruster failures,” in *2016 IEEE International Conference on Robotics and Automation (ICRA)*. IEEE, 2016, pp. 2625–2630.
- [16] Y.-s. Sun, X.-r. Ran, Y.-m. Li, G.-c. Zhang, and Y.-h. Zhang, “Thruster fault diagnosis method based on gaussian particle filter for autonomous underwater vehicles,” *International*

- Journal of Naval Architecture and Ocean Engineering*, vol. 8, no. 3, pp. 243–251, 2016.
- [17] A. Caiti, F. Di Corato, F. Fabiani, D. Fenucci, S. Grechi, and F. Pacini, “Enhancing autonomy: Fault detection, identification and optimal reaction for over-actuated auvs,” in *OCEANS 2015-Genova*. IEEE, 2015, pp. 1–6.
  - [18] M. Caccia, R. Bono, G. Bruzzone, G. Bruzzone, E. Spirandelli, and G. Veruggio, “Experiences on actuator fault detection, diagnosis and accommodation for rovs,” *International Symposium of Unmanned Untethered Submersible Technol*, pp. 3–21, 2001.
  - [19] B. Y. Raanan, J. Bellingham, Y. Zhang, B. Kieft, M. J. Stanway, R. McEwen, and B. Hobson, “A real-time vertical plane flight anomaly detection system for a long range autonomous underwater vehicle,” in *OCEANS 2015 - MTS/IEEE Washington*, 2015, pp. 1–6.
  - [20] V. Chandola, A. Banerjee, and V. Kumar, “Anomaly detection: A survey,” *ACM computing surveys (CSUR)*, vol. 41, no. 3, pp. 1–58, 2009.
  - [21] K. Szwaykowska and F. Zhang, “Controlled lagrangian particle tracking: error growth under feedback control,” *IEEE Transactions on Control Systems Technology*, vol. 26, no. 3, pp. 874–889, 2017.
  - [22] S. Cho, F. Zhang, and C. R. Edwards, “Learning and detecting abnormal speed of marine robots,” *International Journal of Advanced Robotic Systems*, vol. 18, no. 2, p. 1729881421999268, 2021.
  - [23] B. T. Morris and M. M. Trivedi, “A survey of vision-based trajectory learning and analysis for surveillance,” *IEEE transactions on circuits and systems for video technology*, vol. 18, no. 8, pp. 1114–1127, 2008.
  - [24] P.-R. Lei, “A framework for anomaly detection in maritime trajectory behavior,” *Knowledge and Information Systems*, vol. 47, no. 1, pp. 189–214, 2016.
  - [25] O. Rosen and A. Medvedev, “An on-line algorithm for anomaly detection in trajectory data,” in *2012 American Control Conference (ACC)*. IEEE, 2012, pp. 1117–1122.
  - [26] O. Schofield, J. Kohut, D. Aragon, L. Creed, J. Graver, C. Haldeman, J. Kerfoot, H. Roarty, C. Jones, D. Webb, and S. Glenn, “Slocum gliders: Robust and ready,” *Journal of Field Robotics*, vol. 24, no. 6, pp. 473–485, 2007.
  - [27] D. Chang, F. Zhang, and C. R. Edwards, “Real-time guidance of underwater gliders assisted by predictive ocean models,” *Journal of Atmospheric and Oceanic Technology*, vol. 32, no. 3, pp. 562–578, 2015.
  - [28] X. Liang, W. Wu, D. Chang, and F. Zhang, “Real-time modelling of tidal current for navigating underwater glider sensing networks,” *Procedia Computer Science*, vol. 10, pp. 1121–1126, 2012.